ORIGINAL PAPER

# Effective Stress and Permeability Redistributions Induced by Successive Roadway and Borehole Excavations

**Shengyong Hu · Fubao Zhou · Yingke Liu · Tongqiang Xia**

**Abstract** Methane extraction from in-seam boreholes is the main approach for recovering methane in China. However, the methane concentration for this method is generally lower than 30 %, which incurs a risk of methane outbursts during pipeline transportation. To increase the methane concentration, we first conducted permeability experiments to investigate the relationships between the permeability and the effective stress at different stages in the complete effective stress–strain process. We then adopted FLAC3D software to calculate the stress distributions around roadways and boreholes after their consecutive excavations and thereby divided the coal mass around the roadway and borehole according to different effective stress stages to understand the gas flow characteristics. The results show that the coal mass along the radial direction of the roadway and borehole can be sequentially divided into four zones, including the full flow zone (FFZ), the transitive flow zone (TFZ), the flow-shielding zone (FSZ), and the in situ rock flow zone (IRFZ), which have been proven correct by field experiments. The methane in the IRFZ was difficult to extract because of the low permeability of coal mass in this zone. The permeability of the FSZ was lower than that of the IRFZ. The permeability along the interface between the FSZ and TFZ was nearly one time as low as that of the IRFZ, while the permeability of the FFZ was two orders of magnitude higher than that of the IRFZ. This four-zone division demonstrates the decaying mechanism of methane extraction concentration and flow in the in-seam borehole and can provide theoretical guidance for improvement of methane extraction.

**Keywords** Coal mine · Methane extraction · Roadway · Borehole · Effective stress · Permeability

S. Hu · F. Zhou (✉)
Key Laboratory of Gas and Fire Control for Coal Mines, China University of Mining and Technology, Xuzhou 221008, Jiangsu, People's Republic of China
e-mail: zfbcumt@gmail.com

S. Hu · F. Zhou · Y. Liu
School of Safety Engineering, China University of Mining and Technology, Xuzhou 221116, Jiangsu, People's Republic of China

T. Xia
State Key Laboratory for Geomechanics and Deep Underground Engineering, China University of Mining and Technology, Xuzhou 221116, Jiangsu, People's Republic of China

## 1 Introduction

More than 95 % of coal mines in China are underground, and 17.6 % of key state-owned coal mines have experienced coal and gas outbursts, which have resulted in great economic and human losses (Yang et al. 2011). In August 2009, the Provisions for Prevention of Coal and Gas Outbursts were enacted in China to reduce outburst accidents (China State Administration of Work Safety 2009). The law highlighted regional methane control measures including mining protective coal seams or preextracting regional methane.

In China, methane preextraction from in-seam methane extraction boreholes has been generally adopted because this process is simple, fast, and cost-effective and has no invalid footage (Karacan et al. 2007). The boreholes are usually drilled along a working face in the excavation process of intake and return airflow roadways. They should be between 10 and 20 m long, sealed, and connected to the extraction pipeline (Fig. 1) (Noack 1998). In addition, the

**Fig. 1** Schematic of the predrainage borehole connection (Noack 1998)
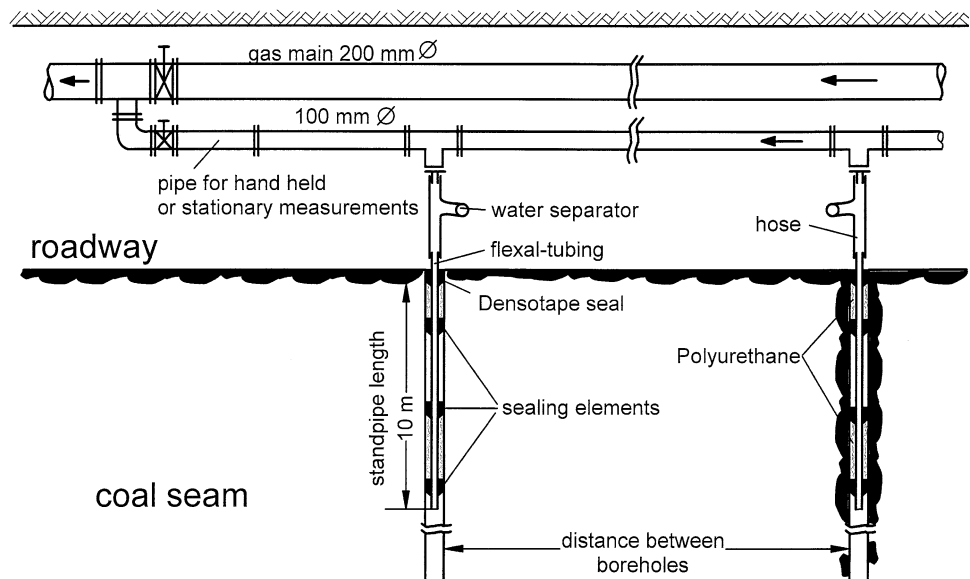
extraction pumps should be able to maintain the pressure in the extraction range below the ambient pressure in the mine. The captured gas is released to the atmosphere, flared, or used in gas-fired turbines to generate electricity.

The methane extraction concentration in most Chinese coal mines is lower than 30 %, which is the minimum concentration based on safety concerns (Wang and Cheng 2012). This value is the internationally accepted standard of a safety factor of at least two times the upper explosive limit (i.e., 30 % or greater methane concentration) for transport and use of gas mixtures (ECE UN, M2M Partnership 2010). Because low-concentration methane is not utilizable and can result in explosions during pipeline transportation, it is usually evacuated. However, this process not only wastes energy but also pollutes the environment (Su and Agnew 2006). Thus, low-concentration methane needs to be controlled.

The methane concentration extracted from in-seam boreholes is directly related to the ability of both the methane in the coal seam and the air in the roadway to flow into boreholes. Permeability is used to describe the resistance of the coal mass to the passage of gas through it (Mordecai and Morris 1974). This parameter is highly sensitive to the stress in the surrounding coal mass (Pan et al. 2010). The stress around the excavated coal mass is strongly affected by roadway and borehole excavation, which changes the permeability of the coal mass.

The relationship between the permeability and stress obtained from permeability experiments in the complete stress–strain process reflects the change in the permeability of coal mass around roadways and boreholes during their deformation and failure. However, most experiments to date have only revealed the changes in rock mass

permeability during its deformation and failure (Schulze et al. 2001; Oda et al. 2002; Wang and Park 2002; Alkan et al. 2007; Yang et al. 2007; Zhang et al. 2007), whereas few studies have examined the changes in coal mass permeability during its deformation and failure (Cao et al. 2011; Wang et al. 2013).

Jayanthu et al. (2004) presented field observations on the distribution of vertical stress in a thick coal seam during pillar extraction. Hao and Azzam (2005) provided a graphical distribution of plastic zones around underground openings in rock masses with a fault. Lee and Bassett (2007) proposed the influence zones in a two-dimensional (2-D) pile–soil–tunneling interaction based on their model test and numerical analysis. Kwon et al. (2009) investigated the characteristics of the damaged zone developed during the construction of an underground research tunnel. Islam and Shinjo (2009) used their two-dimensional boundary-element method to numerically simulate and analyze stress distributions around an entry roadway. Wang et al. (2009) used their realistic failure process analysis code to compute the extent of the damaged/disturbed zone due to excavation. Gao et al. (2012) presented an analytic method for analyzing stress and plastic zones of surrounding rock in cold region tunnels. Aadnoy (1989) presented the anisotropic stress equations that can be used to solve fracturing problems for horizontal boreholes. Wang and Sterling (2007) used finite-element analysis to numerically compute the yield zone size around a borehole. Gaede et al. (2012) investigated borehole stresses in anisotropic media. However, all of these studies mainly focused on the stress distribution induced by single roadway or borehole drilling. Very few works have studied the effective stress redistributions induced by successive roadway and borehole drillings.

In this work, we first conducted permeability experiments to investigate the relationship between the effective stress and permeability during coal deformation and the failure of a completely effective stress–strain process. We then applied FLAC3D software to study the stress changes in the coal mass after successive roadway and borehole drillings. Third, we calculated the methane pressure distributions around roadways and boreholes after their consecutive excavations. Fourth, we plotted and divided the coal masses around roadways and boreholes into four zones according to the experimental relationship and the numerical simulation. Finally, we conducted field experiments to verify this four-zone division.

## 2 Research Background

The No. 8 Coal Mine of Pingdingshan is the first oversized mine in China. However, this mine has also experienced multiple serious incidents. In its history, 36 coal and gas outbursts have occurred, among which 17 outbursts occurred at its No. 15 seam. Working face 13,330 of the seam spans 1,300 and 186 m in strike and dip length, respectively, and the seam is approximately 3 m thick on average. The methane pressure in the coal seam ranges from 0.9 to 1.3 MPa, and the methane content ranges from 18 to 20 m$^3$/ton. This area is part of a low-permeability coal seam that is at great risk for coal and gas outbursts.

Methane preextraction from in-seam boreholes along the inclination of the coal bed roadway was implemented to eliminate this risk as soon as possible and reduce the emission rate of coal bed gas toward the working face during excavation; Fig. 2 shows the layout of the roadways and the boreholes. The roadway distributes more than 900 boreholes, each of which is 90–110 m deep, with a total length of more than 90,000 m along the intake and return airflow. At present, approximately 600 boreholes have been extracted over less than 1 month, and their methane concentrations have been reduced to lower than 30 %. Therefore, extraction has been stopped for the majority of boreholes.

## 3 Experiments

### 3.1 Experimental Approach

The experimental apparatus is shown in Fig. 3. The loading system supplies axial and confining pressures on the coal sample installed in the pressure chamber. The pressure of the gas source after being boosted by a pneumatic booster pump is maintained stable again by the gas pressure regulator device. The air compressor supplies the power to the

pneumatic booster. The pressure sensor and the mass flow meter are used to measure the gas pressure and gas flow in the permeation process.

The coal mass used in the experiment was chosen from working face 13,330 of the No. 8 Coal Mine of Pingdingshan, Henan Province, China. The coal samples were further processed into cylinders of 50 mm diameter and 100 mm length. The gas was 99.9 % pure methane. The confining pressure and the gas pressure were set at 10 and 1 MPa, respectively. The experimental procedure was as follows:

1. Coal sample no. 1 was placed on the osmotic pressure indenter; the tube was continuously and uniformly heat-shrunk with a hairdryer to tensely wrap the indenter end and the coal sample. The well-fitted sample was placed on the indenter located at the bottom of the testing machine and connected to the gas pipelines.
2. The pressure chamber was lowered, and hydrostatic pressure was applied to the coal sample to 10 MPa at 3 MPa/min; the axial and confining pressures were maintained constant, and methane was gradually injected to increase the pressure with an increment of 0.25 MPa. After reaching 1.1 MPa, the pressure at the inlet end was maintained stable. Once the methane was completely adsorbed, the valve at the outlet end was opened, and its pressure was maintained at 0.1 MPa; when the gas flow was stable, the initial gas flow was recorded.
3. The confining pressure was maintained constant, and the force control mode was used to load the axial pressure at a speed of 10 kN/min. After the coal sample yielded, the circular displacement control mode was used to continuously load at a speed of 0.04 mm/min. Prior to the axial peak load, the axial and confining pressures were maintained constant at every axial load of 6 kN. The gas flow was recorded when it reached steady state, and the load was continued. After the axial peak load, the axial load was reduced by 2 kN each time while maintaining the axial confining pressures constant. When the gas flow reached steady state, it was recorded and loading was continued.
4. When the coal sample reached the residual stage, the test was concluded and the above steps were repeated with sample no. 2.

The gas permeability is defined by Darcy's equation as follows:

$$k = \frac{2Q_0 P_0 \mu L}{A(P_1^2 - P_2^2)}, \tag{1}$$

where $k$ is the gas permeability (m$^2$), $Q_0$ is the volumetric flow rate at the reference pressure (m$^3$/s), $\mu$ is the gas
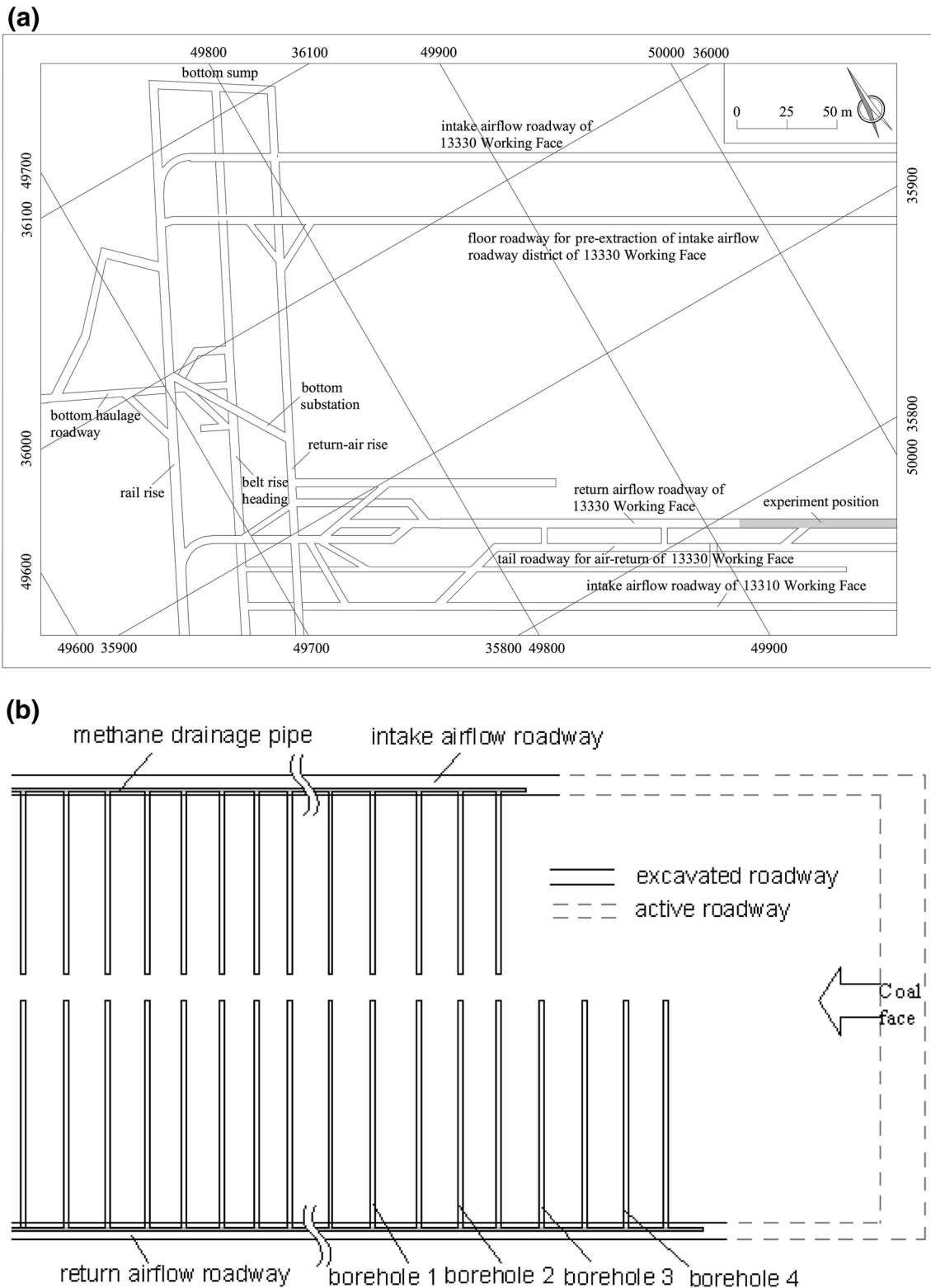
**(a)**



**(b)**



Fig. 2 Layout of the **a** roadways and **b** boreholes

viscosity (Pa s), $L$ is the length of the coal sample (m), $P_0$ is the reference pressure (Pa), $A$ is the cross-sectional area of the coal sample (m$^2$), $P_1$ is the upstream gas pressure (Pa), and $P_2$ is the downstream gas pressure (Pa). In this paper, the permeability $k$ is defined in SI units of m$^2$. The conversion factor from m$^2$ to mD is expressed by
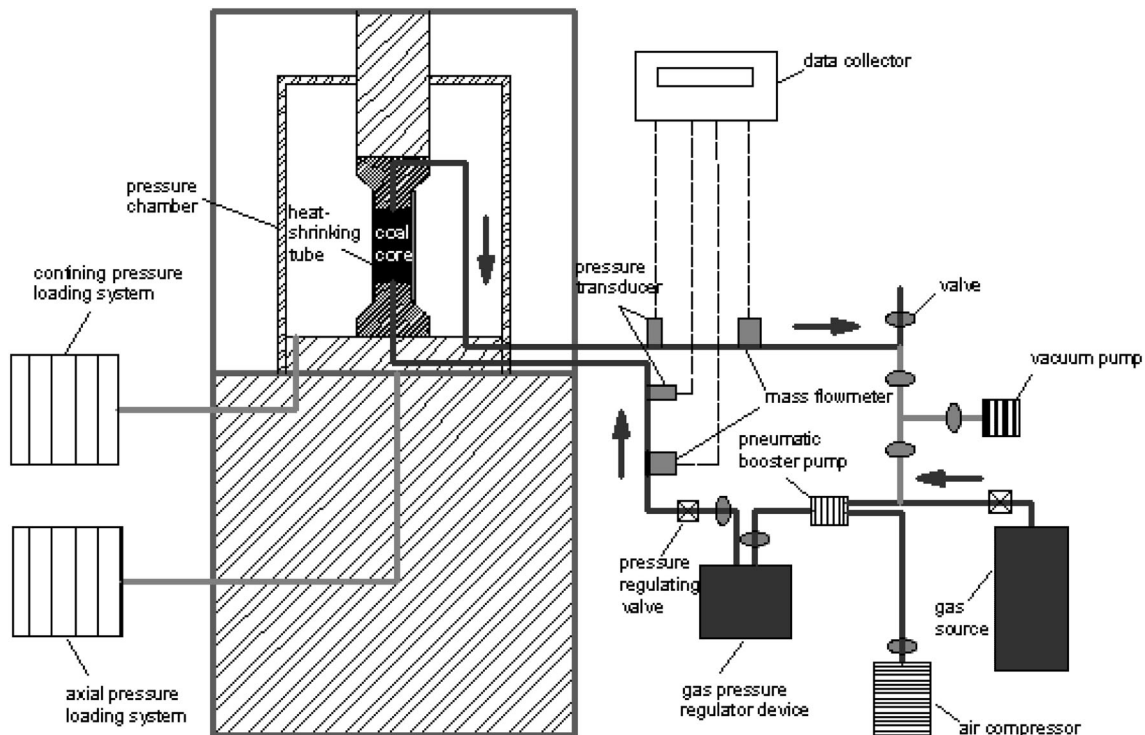
**Fig. 3** Schematic of the experimental system

1 mD $= 10^{-15}$ m$^2$. Based on the measured parameters, such as the gas flow at the outlet end and the pressures at both ends of the coal sample, the gas permeability is calculated by using Eq. (1).

### 3.2 Relationship Between Effective Stress and Permeability

We obtained the relationships between the permeability and the effective stress at different effective stress stages in the complete effective stress–strain process from permeability experiments. Figure 4 shows the changes in both the effective stress and permeability with axial strain for coal samples no. 1 and 2 subjected to methane pressure of 1 MPa. Figure 4 clearly shows that the effective stress–strain curve agrees well with the methane permeability–strain curve and can be grossly divided into four different stages. Stage I is the initial compression stage, stage II is the elastic deformation stage, stage III is the yielding failure stage, and stage IV is the fracture interconnectivity stage.

In stage I, the gas permeability decreases due to closure of original pores and microcracks in the coal sample. In stage II, the original pores and cracks inside the coal sample close further. As a result, only elastic deformation occurs in the coal sample, which narrows the gas flow paths. Therefore, the permeability further decreases. During stages I and II, the permeability decreases as the stress

increases. At the interface between stage II and stage III, the coal sample yields, and the permeability reaches a minimum (Cao et al. 2011), which indicates that the pores and fractures inside the coal sample are minimized. Therefore, the paths through which methane flows are at their narrowest. During stage III, the permeability dramatically increases, which suggests that the coal sample starts to fail. Its original fractures are expanding, a significant number of new microcracks are produced, and macrocracks are formed. At this stage, the paths through which methane flows gradually become smooth, and the permeability increases rapidly and exceeds those at stages I and II. During the transition to stage IV, the permeability continues to rise, which indicates that dislocations appear along the surfaces inside the fractured coal mass, the degrees of crack expansion and coalescence increase, and cracks are well developed.

Previous experimental measurements indicated that the permeability of coal decreases exponentially as the effective stress increases (Somerton et al. 1975; Durucan and Edwards 1986). In contrast to this paper, the effective stress–permeability relationship was considered to be a piecewise exponential function in this previous work. As shown in Fig. 5, the permeability during stage IV increases much faster than in stages I and II as the effective stress decreases. Prior to the drilling of roadways and boreholes, the coal mass is in stage II, and its effective stress is 16 MPa. Therefore, the original permeability is
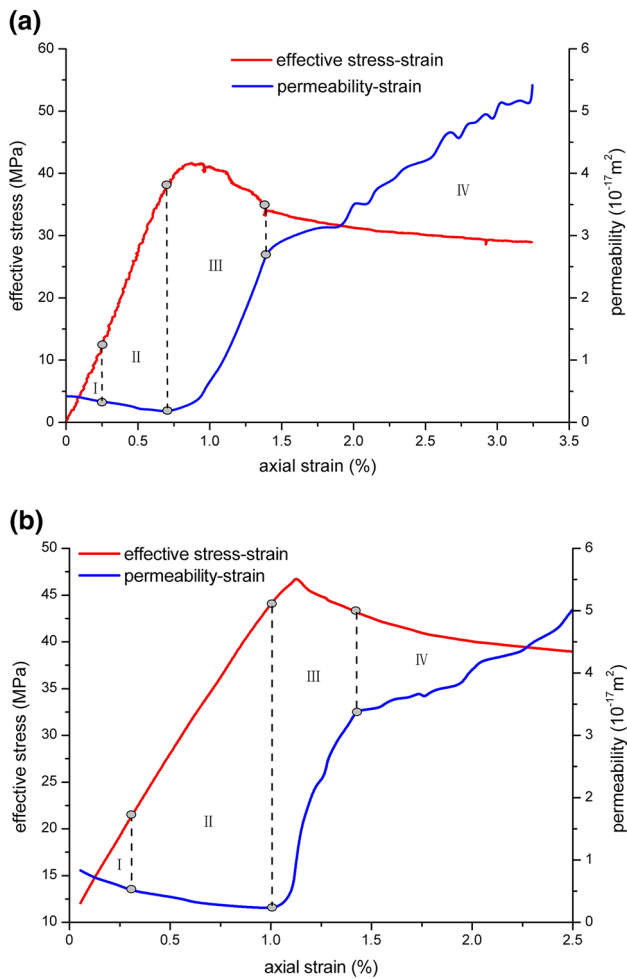
Fig. 4 Effective stress and permeability versus axial strain in the complete effective stress–strain process: **a** sample no. 1 and **b** sample no. 2
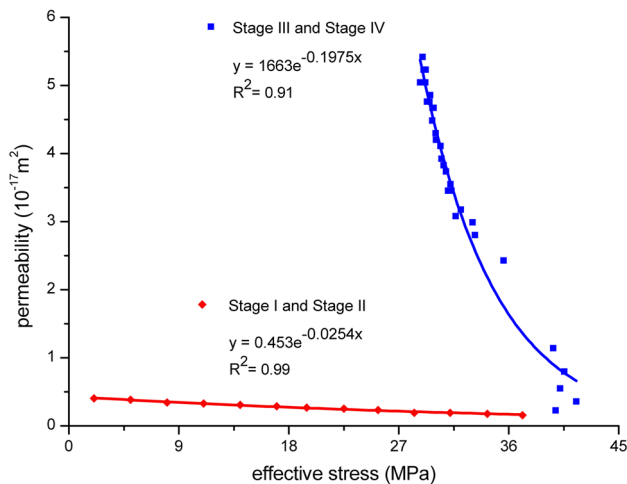


Fig. 5 Relationship between the permeability and effective stress for coal sample no. 1

0.0030 mD. The permeability of the interface between stage I and stage II is 0.0017 mD, which is approximately half the original permeability. After a roadway or borehole is drilled, the surrounding coal mass consecutively passes through stage II, stage III, and stage IV in the complete effective stress–strain curve. When the effective stress again reaches 16 MPa, the permeability is 0.70554 mD, which is two orders of magnitude higher than its original value.

If the coal mass around a roadway or borehole can be divided according to the different effective stress stages, the distribution of the permeability of the surrounding coal mass can be determined.

## 4 Numerical Modeling

### 4.1 Description of the Model

After having obtained the relationships between the permeability and effective stress at different effective stress stages as described above, the stresses and methane pressures for the coal mass surrounding the roadway and borehole after excavation must still be calculated to divide the effective stress stages corresponding to the different coal masses around the roadway and borehole and to determine the gas flow characteristics of these coal mass zones.

FLAC3D software was used to investigate the stress changes after successive roadway and borehole drillings. As an explicit three-dimensional (3-D) finite-difference program, it has been extensively used in geotechnical, mining, hydraulic, and geological engineering projects to simulate the behaviors of 3-D structures of soil, rock or other materials subject to plastic flow when their yield limits are reached (Yasitli and Unver 2005; Itasca 2006; Whittles et al. 2006, 2007; Chen et al. 2012).

Our model was built according to the geological conditions of working face 13,330 of Pingdingshan Coal Mine. The material properties required by FLAC were measured or estimated from previous engineering reports archived by the coal mine, as listed in Table 1. In Pingdingshan, the ground stress gradient is approximately 0.025 MPa/m. Considering that the top of our model was approximately 640 m below the ground surface, a compressive stress of 16 MPa was loaded on the top of the model as the in situ stress. The initial horizontal stress of the model was 17.92 MPa. Figure 6a shows the stratification of the numerical model with different lithologies. The length, width, and height of the model were 50, 50, and 53 m, respectively. The generalized stratigraphic column that shows the coal seam together with the roof and floor strata is presented in Table 2. In this paper, the cross-section

**Table 1** Initial properties of rock mass

| Lithology | Density (kg/m$^3$) | Bulk modulus (GPa) | Shear modulus (GPa) | Cohesion (MPa) | Friction angle (°) | Tensile strength (MPa) |
|---|---|---|---|---|---|---|
| Siltstone | 2,500 | 23.1 | 10.2 | 7.3 | 40.1 | 3.1 |
| Meso-coarse siltstone | 2,700 | 26.0 | 15.0 | 7.5 | 42.0 | 4.0 |
| Sandy mudstone | 2,450 | 20.1 | 8.0 | 5.2 | 34.0 | 2.0 |
| Coal | 1,400 | 10.0 | 3.0 | 2.0 | 28.0 | 0.8 |
| Fine-grained sandstone | 2,671 | 24.0 | 14.0 | 8.2 | 39.3 | 5.8 |
| Limestone | 2,400 | 19.0 | 6.0 | 4.6 | 31.0 | 1.5 |

shown in Fig. 6b was chosen as our research object. The length, width, and height of the roadway were 50, 4, and 4 m, respectively. The diameter of the borehole was 100 mm, and its depth was only 30 m. Due to the small borehole diameter, the distributions of stress on the other cross-sections were considered to be approximate.

Drilling a roadway or borehole will increase the stress, called the abutment stress or the vertical stress, around the excavated coal mass. The coal mass will deform or fail due to the vertical stress. Most studies of the postexcavation stress distribution have focused on the vertical stress (Steve Zoua et al. 1999; Yasitli and Unver 2005; Cheng et al. 2010; Singh et al. 2011; Jiang et al. 2012; Zhang et al. 2012); for comparison purposes, we still examined the effective stress, i.e., the vertical effective stress, in the following analysis. For convenience, we also did not consider the influence of gas adsorption and desorption on the effective stress distributions after the roadway and borehole were drilled.

### 4.2 Effective Stress Distributions After Successive Roadway and Borehole Excavations

#### 4.2.1 Effective Stress Distributions After Roadway Excavation

The distribution of methane pressure around an excavation body (roadway or borehole) can be described with the following empirical relationship (Borisenko 1985):

$$p = p_i[1 - \exp(-cl^2)], \tag{2}$$

where $p_i$ is the initial pressure (MPa), $c$ is a constant related to the gas permeability of the coal mass (m$^{-2}$), and $l$ is the distance from the edge of the excavation body (m).

Field experience shows that the methane pressure in coal mass not affected by roadway and borehole excavations is equal to the initial pressure (Wang et al. 2007). The constant $c$ could be determined based on this relationship.

As shown in Fig. 7 and Table 3, the coal bed can be divided into three zones according to the effective stress under the influence of roadway excavation: the effective stress-reduced, effective stress-lifted, and in situ effective stress zones. Prior to the effective stress peak position (AC), the coal mass is in the plastic state within 9 m of the roadway. The coal mass within 0–4.9 m (AB), where the effective stress is lower than the in situ effective stress, is in the failure state, and the coal mass after the effective stress peak position (CD) is in the elastic state (Hao et al. 2012; Steve Zoua et al. 1999; Zhang et al. 2012). The coal mass located farther than 26.5 m is still in the in situ state.

As shown in Table 3, the plastic zone (AC) contains the fracture zone (AB) and the plastic enhancement zone (BC). The effective stress from which the coal mass in the fracture zone (AB) suffers is lower than the in situ effective stress. Thus, this zone is also called the effective stress-reduced zone, in which the coal undergoes instability and failure, and the cracks in it are well developed. Furthermore, the region closer to the roadway experiences more serious damage. In the plastic enhancement zone (BC), the coal is in the plastic state, but has a higher carrying capacity. Thus, the effective stress on the coal mass is higher than the in situ effective stress. The elastic zone (outside of AC) includes the elastic deformation zone (CD) and the in situ state zone (outside of AD). Within the elastic deformation zone, the coal subject to the secondary effective stress induced by roadway excavation is still in the elastic deformation state, and the effective stresses at various locations are higher than the in situ effective stress. However, the in situ state zone is not affected by roadway excavation, and the coal remains in the in situ effective stress state.

#### 4.2.2 Effective Stress Distributions After Borehole Excavation

After borehole excavation, four representative observation lines, AB, BC, CD, and AD, were drawn as shown in Fig. 7. These lines are 3, 8, 14, and 29 m away from the roadway, respectively; they are vertical to the borehole directions and originate from the walls of the borehole. Figure 8 shows the relationships of the effective stress and methane pressure to the distance from the borehole wall along various observation lines after borehole excavation. As
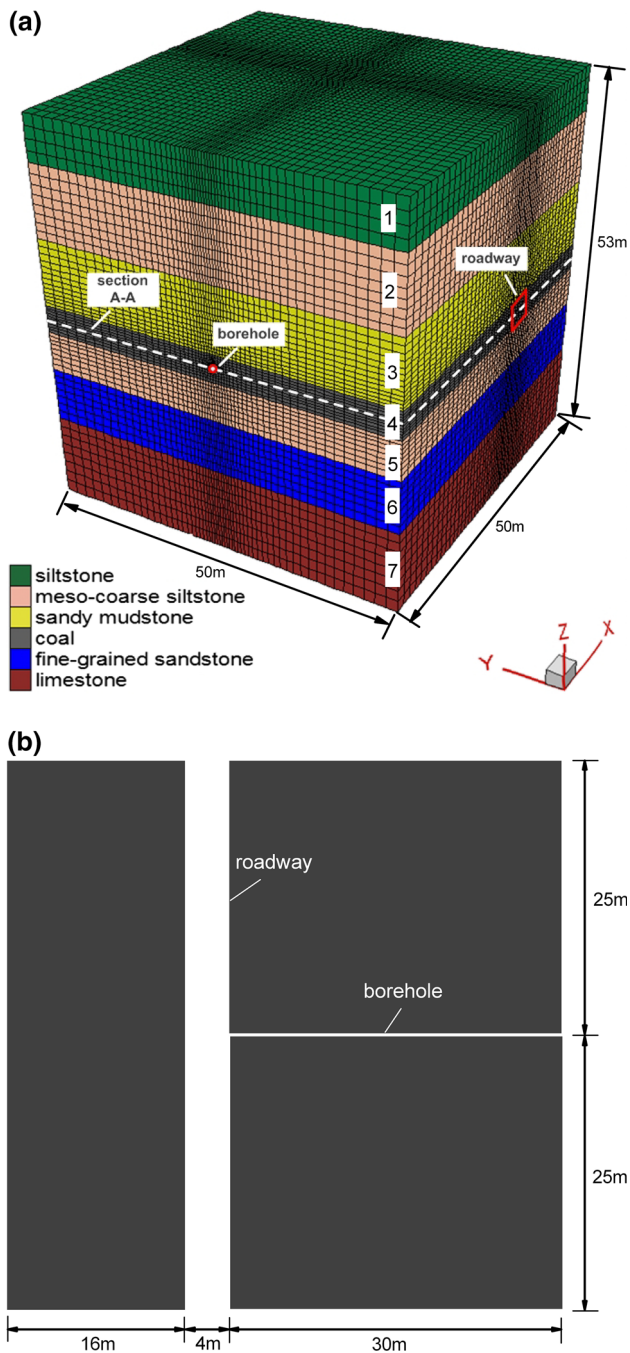
**(a)**



**(b)**



Fig. 6 Numerical simulation model. **a** Model geometry and boundaries. **b** Layout of a roadway and borehole (section A–A)

shown in Fig. 8, the effective stress and methane pressure distributions along the four different observation lines are similar to the changes in the surrounding rock effective stresses and methane pressures after roadway excavation shown in Fig. 7.

After roadway excavation, the effective stress along any of the observation lines is the same and can be considered equal to the initial effective stress prior to borehole excavation. The coal mass in zone $AB$ remains in the failure

state after borehole excavation due to the effect of roadway excavation. The coal mass in zone $BC$ can be considered to be in the failure state due to borehole excavation, as long as the bearing effective stress is lower than that of the initial effective stress. The rest of the coal mass in zone $BC$ remains in the plastic state. The coal mass outside zone $AC$ experiences several states: the mass bearing an effective stress lower than the initial effective stress changes from the elastic state to the failure state, the mass experiencing an effective stress higher than the initial effective stress and located before the peak effective stress changes from the elastic state to the plastic state, and the mass bearing an effective stress positioned after the peak effective stress remains in the elastic state.

The original coal mass on the observation line 29 m away from the roadway is in the elastic state prior to borehole excavation. After borehole excavation, the coal mass in the range of 0–0.29 m away from the borehole reaches the plastic state. In this range, the coal mass within 0–0.20 m suffers from failure. The coal farther than 0.29 m away from the borehole is in the elastic state. Beyond this range, drilling the borehole impacts the coal within 0.29–1.32 m, while the coal more than 1.32 m away from the borehole is not affected by borehole excavation.

The coal mass along the observation line 14 m away from the roadway is in the elastic state prior to borehole excavation. After borehole excavation, the coal within 0–0.35 m away from the borehole reaches the plastic state. In this range, the coal within 0–0.23 m undergoes failure. The coal mass beyond 0.35 m away from the borehole is still in the elastic state. Beyond this, the coal within 0.35–1.35 m away is impacted by the borehole excavation, while that farther away than 1.35 m is not affected.

The coal mass along the observation line 8 m from the roadway is in the plastic enhancement zone after roadway excavation. After borehole excavation, the coal mass between 0 and 0.26 m away from the borehole suffers from failure, while that farther than 0.26 m away remains in the plastic state. In this range, the coal in the 0.26–2.75 m range is affected by borehole excavation, while the coal farther than 2.75 m away is not affected.
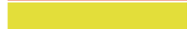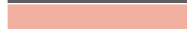
The coal mass along the observation line 3 m away from the roadway remains in the failure state after borehole excavation.

## 5 Classification of Four Zones

### 5.1 Classification of Four Zones After Roadway Excavation

The changes in the permeability of the rock surrounding the roadway can be determined based on the relationship

**Table 2** A generalized stratigraphic column at working face 13,330 (color figure online)

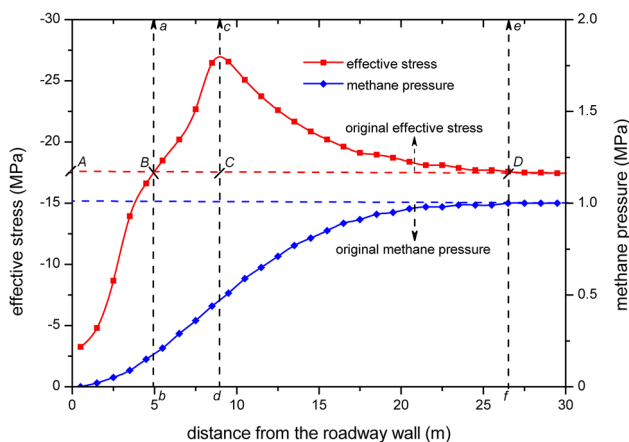| Geological section | Stratum no. | Lithology | Thickness (m) | Depth (m) |
|---|---|---|---|---|
| | 1 | Siltstone | 8 | 648 |
| | 2 | Meso-coarse siltstone | 9 | 657 |
| | 3 | Sandy mudstone | 8 | 665 |
| | 4 | Coal | 4 | 669 |
| | 5 | Meso-coarse siltstone | 7 | 676 |
| | 6 | Fine-grained sandstone | 8 | 684 |
| | 7 | Limestone | 9 | 693 |



**Fig. 7** Relationships between the effective stress and methane pressure versus the distance from the roadway after its excavation. Lines *ab*, *cd*, and *ef* are the boundaries of the zones *AB*, *BC*, and *CD*, respectively
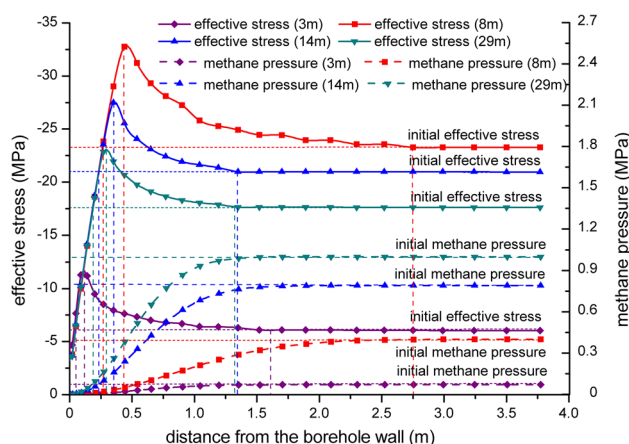


**Fig. 8** Relationships of effective stress and methane pressure to the distance from the borehole after its excavation along various observation lines

between the coal permeability and effective stress shown in Fig. 4, as shown in Fig. 9. Figure 9 clearly shows that the relationship between the permeability of the rock surrounding the roadway and the effective stress agrees well with the relationship between the permeability and the stress given by Jiang et al. (2012). The coal effective stress state in zone *AB* corresponds to stage IV in Fig. 4, and the change in the permeability becomes more dramatic as the effective stress and distance from the roadway decrease. The coal effective stress state in zone *BC* corresponds to stage III in Fig. 4, and the permeability decreases as the distance of the coal mass from the roadway increases. The

permeability is minimized at the effective stress peak position. The coal effective stress state beyond zone *AC* corresponds to stage II in Fig. 4. As the effective stress decreases for the coal in zone *CD*, the permeability gradually increases but remains lower than that of the in situ rock. The coal mass outside zone *AD* is not affected by roadway excavation; its permeability is equal to that of the in situ rock.

Zone *AB* is the full flow zone (FFZ) in which cracks in the coal mass are completely developed and coalesced, forming a flow network. The permeability of the coal in
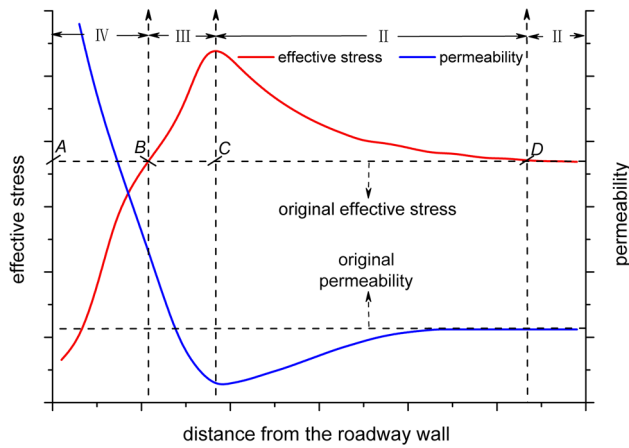
**Table 3** Division of rock surrounding a roadway

| Divided by coal effective stress state | Effective stress–permeability curve phases | Divided by coal flow state | Divided by coal effective stress distribution |
|---|---|---|---|
| Plastic zone (*AC*) | | | |
|   Fracture zone (*AB*) | IV | Full flow zone | Effective stress-reduced zone |
|   Plastic enhancement zone (*BC*) | III | Transitive flow zone | Effective stress-lifted zone |
| Elastic zone (outside *AC*) | | | |
|   Elastic deformation zone (*CD*) | II | Flow-shielding zone | |
|   In situ state zone (outside *AD*) | | In situ rock flow zone | In situ effective stress zone |

Fig. 9 Schematic of the relationship between the permeability and effective stress of rock surrounding the roadway
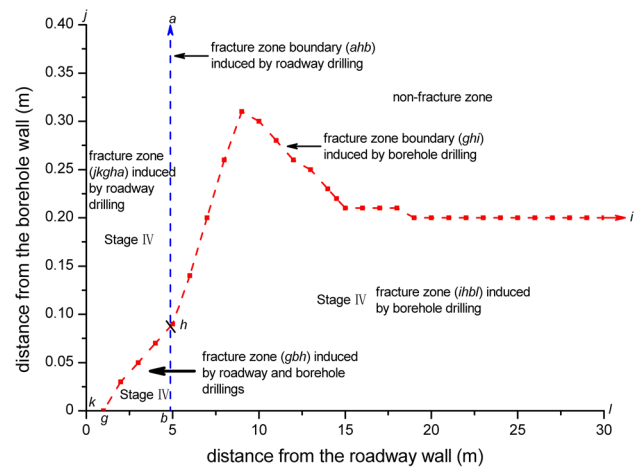


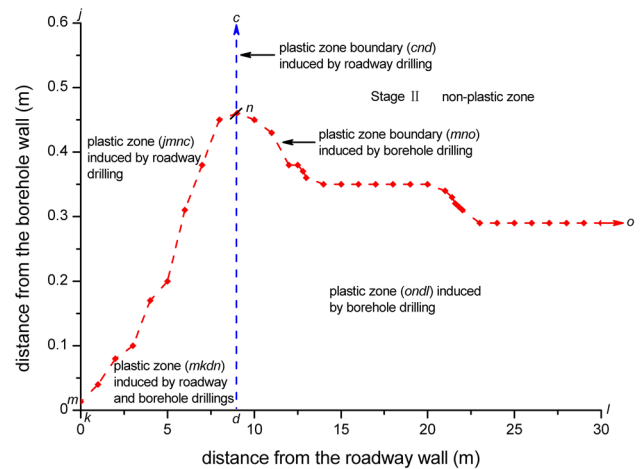Fig. 10 Boundary of fracture zone induced by borehole drilling



Fig. 11 Boundary of plastic zone induced by borehole drilling


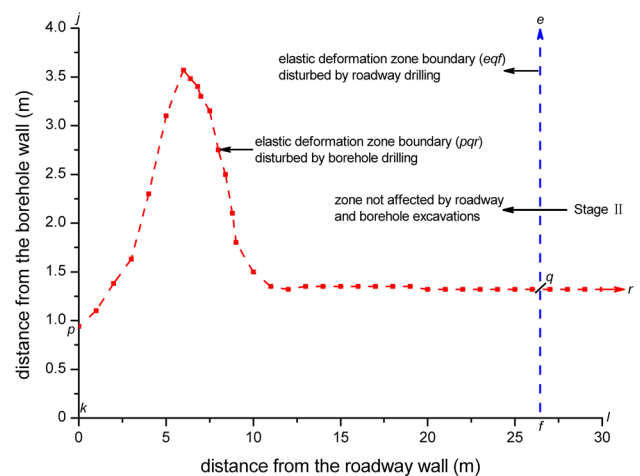
Fig. 12 Boundary of elastic deformation zone induced by borehole drilling

this zone remains high and is two orders of magnitude higher than that of the original coal, which leads to rapid release of methane from this zone into the roadway and a sharp drop in the methane pressure as shown in Fig. 7. Zone BC is the transitive flow zone (TFZ) in which cracks are also well developed, but not completely coalesced. The intrazone permeability rapidly decreases to lower values than that of the in situ rock, reaching its minimum at the interface between zone BC and zone CD. Zone CD is the flow-shielding zone (FSZ) in which the effective stress is higher than that of the in situ rock. The effective stress exerts a pressing impact on pores and cracks in the coal mass and gradually decreases to that of the in situ rock. The coal permeability gradually recovers from the minimum to that of the in situ rock. The coal mass outside zone AD is in the in situ effective stress state. Thus, this zone is the so-called in situ rock flow zone (IRFZ). Because the permeability of zone CD is lower than the original permeability, this zone shields the coal mass outside zone AD from methane to a certain extent and forces the methane pressure in this zone to remain the same as shown in Fig. 7. Therefore, boreholes need to be drilled through zone CD and into the coal mass outside zone AD to drain methane, lower its pressure, and eventually reduce methane emission during coal mining.

## 5.2 Classification of Four Zones After Borehole Excavation

Similar to what Fig. 8 shows, some observation lines were also drawn in Figs. 10, 11, and 12 to show the boundaries of the fracture zone, plastic zone, and elastic deformation zone induced by borehole excavation. The ordinates of these three figures respectively represent the distance to the corresponding boreholes from the ending positions whose

effective stresses are lower than the initial effective stress, the peak effective stress positions, and the distance from the starting positions whose effective stresses are equal to the initial effective stresses along their observation lines. Their abscissas are the distances to the roadway from various observation lines. The boundaries *ghi*, *mno*, and *pqr* of the fracture zone, plastic zone, and elastic deformation zone induced by borehole drilling are defined as the lines connecting all the measured points.

Figure 10 clearly shows that the zone between boundaries *ahi* and *jkl* is the FFZ, in which the coal permeability corresponds to stage IV in Fig. 4. The zone consists of the fracture zones formed by roadway excavation, roadway and borehole excavation, and borehole excavation. Borehole excavation causes the fracture zone produced by roadway excavation to expand along the borehole direction. The width of the FFZ increases from $1.8r$ (borehole radius) at a point 4.9 m away from the roadway, reaches its maximum, $6.2r$, at a point 9 m away from the roadway, and thereafter declines gradually. When the distance from the roadway is greater than 19 m, the width of the fracture zone remains constant at $4.0r$.

The coal permeability in the FFZ is two orders of magnitude higher than that of the original coal mass, and the permeability increases as the distance between the roadway and borehole decreases. The presence of the FFZ around the borehole causes the contained methane to rapidly flow from the coal matrix and drain into the borehole during the initial period of methane extraction, which continuously decreases the methane pressure around the borehole as shown in Fig. 8. Moreover, the air tends to flow in the roadway through the FFZ under the action of negative pressure, which lowers the methane concentration in the borehole and affects the lifetime of borehole methane extraction.

The boundary *cno* in Fig. 11 corresponds to the interface between stage I and stage II in Fig. 4. The permeability of the coal mass at the boundary *cno* is nearly one time as low as that of the in situ coal mass. The boundary is a barrier to gas flow, hindering the permeation of methane from the nonplastic zone into the borehole and complicating methane extraction.

Figure 12 clearly shows that roadway and borehole excavations do not affect the coal mass of the zones farther than 26.5 m away from the roadway and $26.4r$ away from the borehole. Thus, this zone is the IRFZ. In this zone, the methane pressure remains unchanged.

The zone between the boundaries *ahi* and *cno* is the TFZ, as shown in Fig. 13. In this zone, the flow character of the coal mass corresponds to that of stage III in Fig. 4, and the methane in coal in this zone can percolate into the borehole. This zone consists of the plastic enhancement zones produced by the roadway, roadway and borehole,
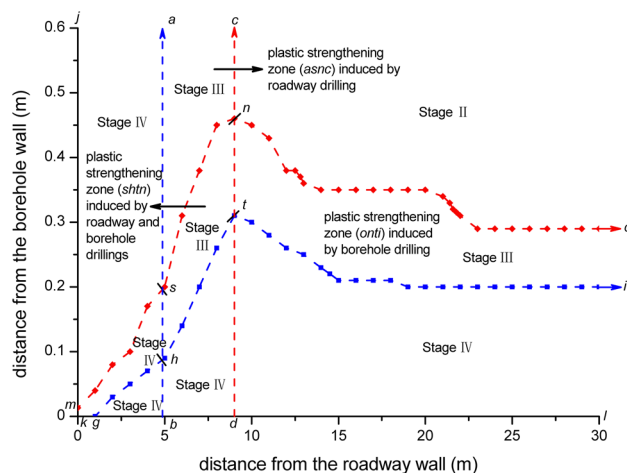


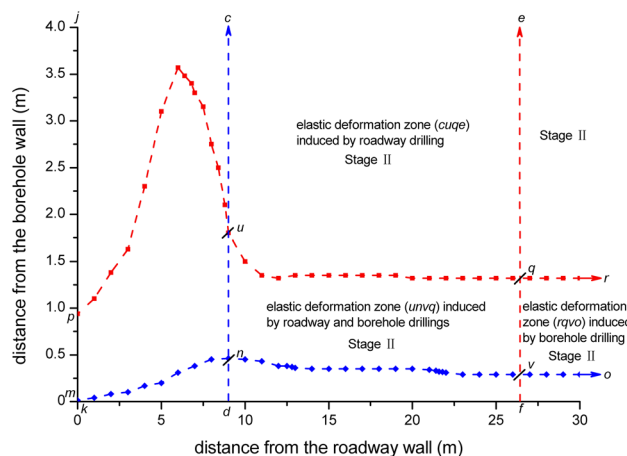**Fig. 13** TFZ distribution after borehole excavation



**Fig. 14** FSZ distribution after borehole excavation

and borehole excavations. The permeability of this zone dwindles gradually from *ahi*, the boundary of the fracture zone, to *cno*, the boundary of the plastic zone. Coal cracks are isolated in this zone, and only some of them are coalesced. Because air in the roadway flows through the FFZ, only a small amount of the air can permeate into the TFZ.

The zone between the boundaries *cno* and *eqr* is the FSZ shown in Fig. 14. This zone consists of three elastic zones produced by the roadway, roadway and borehole, and borehole excavations. The flow characteristics of the coal mass in this zone correspond to those in stage II in Fig. 4, which show increasing flow from *cno* to *eqr*. The permeability in this zone is lower than in the in situ coal. In coal seams with low permeability, the FSZ is a barrier to percolation of in situ coal methane toward the borehole. As extraction continues, the methane pressure continues to decline, and the speed of methane desorption decreases. At this time, an increasing amount of air flows into the borehole from the roadway, which decreases the methane concentration in the borehole.
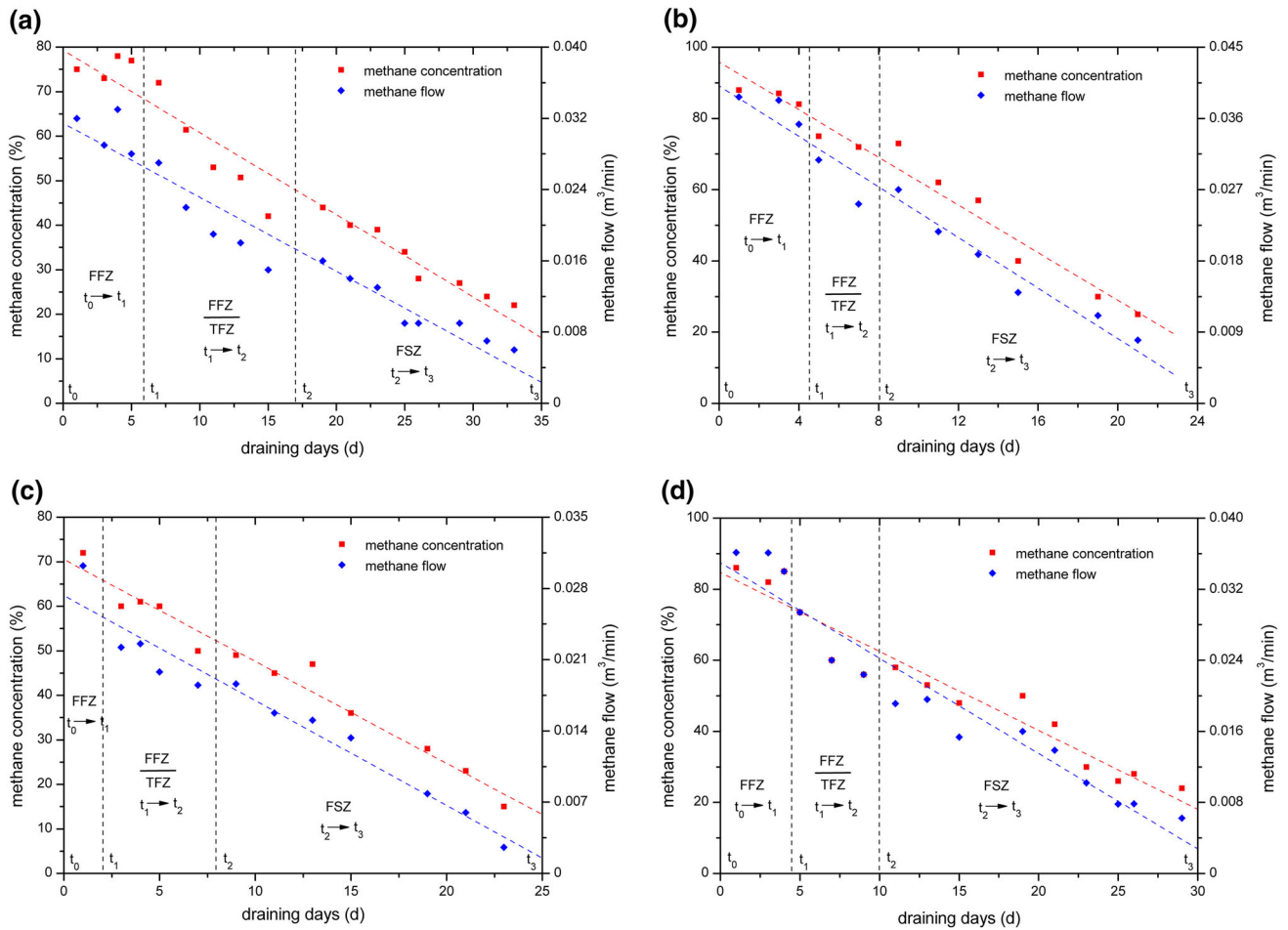
**Fig. 15** Changes in methane concentration and methane flow of: **a** borehole 1, **b** borehole 2, **c** borehole 3, and **d** borehole 4

## 6 Field Experiment

To verify the correctness of the four-zone division, we tested the concentration and flow of methane extraction from in-seam boreholes located at the return airflow roadway of working face 13,330. The layout of the boreholes is shown in Fig. 2b. The borehole suction pressure remained at approximately −15 kPa. The change in the methane concentration and flow in the boreholes could reflect the presence of the four-zone division to some extent. The changes in the methane extraction concentration and flow in the boreholes are shown in Fig. 15a–d.

The flow rate of methane desorbed from the coal mass is determined by the permeability. The methane desorption volume is determined by the methane pressure according to the following relationship:

$$V = V_{\mathrm{L}}\left(\frac{P_0}{P_{\mathrm{L}} + P_0} - \frac{Pt_i}{P_{\mathrm{L}} + Pt_i}\right), \tag{3}$$

where $V_{\mathrm{L}}$ represents the Langmuir volume (cm³/g), $P_{\mathrm{L}}$ represents the Langmuir pressure (Pa), $P_0$ represents the

initial methane pressure (Pa), and $P_{t_i}$ represents the methane pressure at time $t_i$ (Pa).

A comparison of the four zones and the methane pressure in the coal mass along the radial direction of a borehole is shown in Fig. 16. Based on Fig. 16 and Eq. (3), we analyze Fig. 15a–d as follows: from $t_0$ to $t_1$, the methane pressure in the FFZ begins to decline, which leads to methane desorption. Because the permeability of the coal mass in this zone is considerable, the desorbed methane rapidly flows into the borehole. Moreover, the air in the roadway cannot easily flow into the borehole because the methane pressure is much higher than the air pressure, all of which results in higher methane concentration and flow in the borehole. From $t_1$ to $t_2$, the methane pressures in the FFZ and TFZ both begin to decline. The methane desorption in the FFZ is nearly complete, and the methane desorbed in the TFZ flows through the FFZ to the borehole, while a small amount of air begins to flow into the borehole, which decreases the methane concentration and flow. From $t_2$ to $t_3$, methane desorption in the FFZ and TFZ becomes increasingly difficult, while the coal permeability
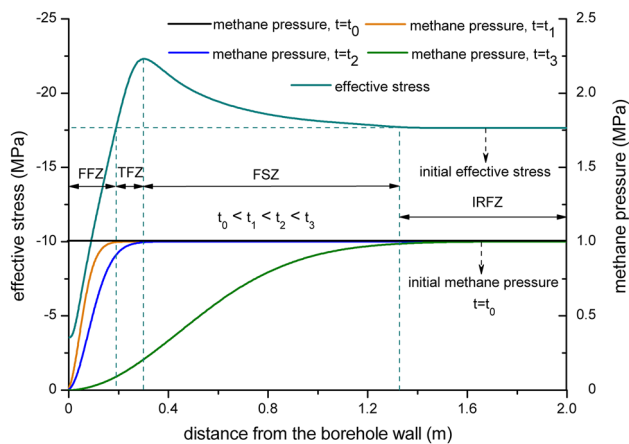
**Fig. 16** Relationships of effective stress and methane pressure to distance from the borehole partitioned according to the four-zone division. *t* represents draining days

in the FSZ is lower than that in the IRFZ, which hinders the flow of methane into the borehole from both the FSZ and IRFZ and results in the easy passage of air in the roadway through the FFZ into the borehole to ultimately rapidly lower the methane concentration and flow in the borehole.

The above analysis shows that the FFZ plays a dominant role in the effect on the methane concentration and flow enhancements from $t_0$ to $t_1$, both the FFZ and TFZ combine to control the methane concentration and flow from $t_1$ to $t_2$, whereas the FSZ dominates the outflow of methane and the inflow of roadway air from $t_2$ to $t_3$. Therefore, the field experiment proved that the division into four zones is acceptable and can be used to guide methane extraction.

Filling fractures in the FFZ with fine particles (Zhou et al. 2009) could effectively seal leaking fractures around the borehole and greatly increase the methane extraction concentration, which provides direct evidence for the presence of the FFZ. The water jets in both the water jet technique (Lu et al. 2009) and high-pressure pulsed water jet technique (Lu et al. 2010) are capable of penetrating the FSZ through the FFZ and IRFZ. Both techniques could greatly increase the methane flow, which constitutes additional indirect evidence for the existence of the FSZ.

## 7 Conclusions

The entire coal deformation and failure process can be divided into four stages in the order of the initial compression stage, elastic deformation stage, yielding failure stage, and fracture interconnectivity stage. The permeability of the coal mass during the initial compression and elastic deformation stages decreases as the effective stress increases and is minimized at the interface of the elastic deformation stage and the yielding failure stage. At the yielding failure stage, the permeability increases rapidly and exceeds that at the initial compression stage. At the fracture interconnectivity stage, the permeability continues to increase as the effective stress decreases.

After roadway excavation, three zones, including the FFZ, TFZ, and FSZ, are consecutively formed along the radial direction of the roadway. After borehole excavation, these zones expand along the borehole direction. Their flow characteristics correspond to those at the fracture interconnectivity stage, yielding failure stage, and elastic deformation stage during coal deformation and failure. The permeability of the coal mass at the interface of the TFZ and FSZ is minimized at a value two times lower than that of the original coal mass. The coal permeability in the FFZ remains at a high level and is two orders of magnitude higher than that of the original coal.

During the initial stage of methane extraction, the methane in the FFZ can rapidly flow into the borehole due to the high permeability and can lead to a higher methane concentration and flow. As extraction continues, the rate of methane desorption in the FFZ and TFZ decreases, and the FSZ prevents the methane in the original coal from flowing into the borehole, both of which result in a rapid decrease of the methane flow. Moreover, the air from the roadway under the negative pressure tends to rapidly flow into the borehole, which rapidly decreases the methane concentration.

## References

Aadnoy BS (1989) Stresses around horizontal boreholes drilled in sedimentary rocks. J Petrol Sci Eng 2:349–360

Alkan H, Cinar Y, Pusch G (2007) Rock salt dilatancy boundary from combined acoustic emission and triaxial compression tests. Int J Rock Mech Min 44:108–119

Borisenko AA (1985) Effect of gas pressure on stresses in coal strata. J Min Sci 21:88–92

Cao SG, Guo P, Zhang ZG, Li Y, Wang Y (2011) Seepage laws of two kinds of disastrous gas in complete stress-strain process of coal. Min Sci Technol 21:851–856

Chen JH, Wang T, Zhou Y, Zhu YL, Wang XX (2012) Failure modes of the surface venthole casing during longwall coal extraction: a case study. Int J Coal Geol 90–91:135–148

Cheng YM, Wang JA, Xie GX, Wei WB (2010) Three-dimensional analysis of coal barrier pillars in tailgate area adjacent to the fully mechanized top caving mining face. Int J Rock Mech Min 47:1372–1383

China State Administration of Work Safety (2009) Specification of coal and gas outburst prevention. China Coal Industry Press, Beijing

Durucan S, Edwards JS (1986) The effects of stress and fracturing on permeability of coal. Min Sci Technol 3:205–216

Gaede O, Karpfinger F, Jocker J, Prioul R (2012) Comparison between analytical and 3D finite element solutions for borehole stresses in anisotropic elastic rock. Int J Rock Mech Min 51:53–63

Gao GY, Chen QS, Zhang QS, Chen GQ (2012) Analytical elasto-plastic solution for stress and plastic zone of surrounding rock in cold region tunnels. Cold Reg Sci Technol 72:50–57

Hao YH, Azzam R (2005) The plastic zones and displacements around underground openings in rock masses containing a fault. Tunn Undergr Sp Tech 20:49–61

Hao ZY, Lin BQ, Gao YB, Cheng YY (2012) Establishment and application of drilling sealing model in the spherical grouting mode based on the loosing-circle theory. Min Sci Technol 22:895–898

Islam MR, Shinjo R (2009) Numerical simulation of stress distributions and displacements around an entry roadway with igneous intrusion and potential sources of seam gas emission of the Barapukuria coal mine, NW Bangladesh. Int J Coal Geol 78:249–262

Itasca Consulting Group Inc (2006) FLAC3D-fast Lagrangian analysis of continua in 3 dimensions. Ver. 3.1 user's manual. ICG, Minneapolis

Jayanthu S, Singh TN, Singh DP (2004) Stress distribution during extraction of pillars in a thick coal seam. Rock Mech Rock Eng 37:171–192

Jiang YD, Wang HW, Xue S, Zhao YX, Zhu J, Pang XF (2012) Assessment and mitigation of coal bump risk during extraction of an island longwall panel. Int J Coal Geol 95:20–33

Karacan CÖ, Daimond WP, Schaltzel SJ (2007) Numerical analysis of the influence of in-seam horizontal methane drainage boreholes on longwall face emission rates. Int J Coal Geol 72:13–32

Kwon S, Lee CS, Cho SJ, Jeon SW, Cho WJ (2009) An investigation of the excavation damaged zone at the KAERI underground research tunnel. Tunn Undergr Sp Tech 24:1–13

Lee Y-J, Bassett RH (2007) Influence zones for 2D pile–soil-tunneling interaction based on model test and numerical analysis. Tunn Undergr Sp Tech 22:325–342

Lu TK, Yu H, Zhou TY, Mao JS, Guo BH (2009) Improvement of methane drainage in high gassy coal seam using waterjet technique. Int J Coal Geol 79:40–48

Lu YY, Liu Y, Li XH, Kang Y (2010) A new method of drilling long boreholes in low permeability coal by improving its permeability. Int J Coal Geol 84:94–102

ECE UN, M2M Partnership (2010) Best practice guidance for effective methane drainage and use in coal mines. United Nations, New York

Mordecai M, Morris LH (1974) The effect of stress on the flow of gas through coal measure strata. Min Eng 133:435–443

Noack K (1998) Control of gas emissions in underground coal mines. Int J Coal Geol 35:57–82

Oda M, Takemura T, Aoki T (2002) Damage growth and permeability change in triaxial compression tests of Inada granite. Mech Mater 34:313–331

Pan ZJ, Connell LD, Camilleri M (2010) Laboratory characterization of coal reservoir permeability for primary and enhanced coalbed methane recovery. Int J Coal Geol 82:252–261

Schulze O, Popp T, Kern H (2001) Development of damage and permeability in deforming rock salt. Eng Geol 61:163–180

Singh AK, Singh R, Maiti J, Rakesh K, Mandal PK (2011) Assessment of mining induced stress development over coal pillars during depillaring. Int J Rock Mech Min 48:805–818

Somerton WH, Söylemezoglu IM, Dudley RC (1975) Effect of stress on permeability of coal. Int J Rock Mech Min Sci Geomech Abstr 12:129–145

Steve Zoua DH, Yu CX, Xian XF (1999) Dynamic nature of coal permeability ahead of a longwall face. Int J Rock Mech Min 36:693–699

Su S, Agnew J (2006) Catalytic combustion of coal mine ventilation air methane. Fuel 85:1201–1210

Wang L, Cheng YP (2012) Drainage and utilization of Chinese coal mine methane with a coal-methane co-exploitation model: analysis and projections. Resour Policy 37:315–321

Wang J-A, Park HD (2002) Fluid permeability of sedimentary rocks in a complete stress-strain process. Eng Geol 63:291–300

Wang X, Sterling RL (2007) Stability analysis of a borehole wall during horizontal directional drilling. Tunn Undergr Sp Tech 22:620–632

Wang ZF, Yang LP, Tian KY, Ma GL (2007) Methods to define laneways loose zone of tick coal seam with enriched gas and spontaneous combustion. Safety Coal Mine 02:1–3

Wang SH, Lee CI, Ranjith PG, Tang CA (2009) Modeling the effects of heterogeneity and anisotropy on the excavation damaged/disturbed zone (EDZ). Rock Mech Rock Eng 42:229–258

Wang SG, Elsworth D, Liu JS (2013) Permeability evolution during progressive deformation of intact coal and implications for instability in underground coal seams. Int J Rock Mech Min 58:34–45

Whittles DN, Lowndes IS, Kingman SW, Yates C, Jobling S (2006) Influence of geotechnical factors on gas flow experienced in a UK longwall coal mine panel. Int J Rock Mech Min 43:369–387

Whittles DN, Lowndes IS, Kingman SW, Yates C, Jobling S (2007) The stability of methane capture boreholes around a long wall coal panel. Int J Coal Geol 71:313–328

Yang TH, Liu J, Zhu WC, Elsworth D, Tham LG, Tang CA (2007) A coupled flow-stress-damage model for groundwater outbursts from an underlying aquifer into mining excavations. Int J Rock Mech Min 44:87–97

Yang W, Lin BQ, Qu YA, Zhao S, Zhai C, Jia LL, Zhao WQ (2011) Mechanism of strata deformation under protective seam and its application for relieved methane control. Int J Coal Geol 85:300–306

Yasitli NE, Unver B (2005) 3D numerical modeling of longwall mining with top-coal caving. Int J Rock Mech Min 42:219–235

Zhang J, Standifird WB, Roegiers J-C, Zhang Y (2007) Stress-dependent fluid flow and permeability in fractured media: from lab experiments to engineering applications. Rock Mech Rock Eng 40:3–20

Zhang RL, Wang ZJ, Chen JW (2012) Experimental research on the variational characteristics of vertical stress of soft coal seam in front of mining face. Safety Sci 50:723–727

Zhou FB, Li JH, Ze X, Liu YK, Zhang RG, Shen SJ (2009) A study of the second hole sealing method to improve gas drainage in coal seams. Min Sci Technol 38:764–768